Chitosan with the addition of zeolite and ZnO nanoparticles as a new antibacterial agent

Mohsen Safaei[1), 2)] (ORCID ID: 0000-0003-3885-6640), **Mohammad Salmani Mobarakeh**[2)] (0000-0002-3272-4041), **Hamid Reza Mozaffari**[2), 3)] (0000-0001-9351-1499), **Ling Shing Wong**[4)] (0000-0002-5869-0804), **Nima Fallahnia**[2), 5), *)] (0000-0002-9571-6137)

DOI: https://doi.org/10.14314/polimery.2024.10.2

Abstract: Chitosan/zeolite/ZnO nanocomposites with different contents of components were obtained using the Taguchi method. Based on the conducted studies, optimal conditions for the synthesis of the nanocomposite (7.5 mg/mL chitosan, 0.2 mg/mL zeolite and 9 mg/mL ZnO) with the best antibacterial properties (no growth of *S. mutans*) were established. Spectroscopic, microscopic, thermal, and antibacterial methods were used to characterize the nanocomposite and its components in relation to *S. mutans* biofilm. The chitosan/zeolite/ZnO nanocomposite can be used as an effective antibacterial compound in various applications due to its structural and antibacterial properties.

Keywords: human health, antibacterial effect, nanocomposites, chitosan, zeolite, zinc oxide.

Chitozan z dodatkiem zeolitu i nanocząstek ZnO jako nowy środek antybakteryjny

Streszczenie: Metodą Taguchi otrzymano nanokompozyty chitozan/zeolit/ZnO o różnej zawartości chitozanu, zeolitu i ZnO. Na podstawie przeprowadzonych badań ustalono optymalne warunki syntezy nanokompozytu (7,5 mg/mL chitozanu, 0,2 mg/mL zeolitu i 9 mg/mL ZnO) o najlepszych właściwościach przeciwbakteryjnych (brak wzrostu bakterii *S. mutans*). Do scharakteryzowania nanokompozytu i jego składników w odniesieniu do biofilmu *S. mutans* zastosowano metody spektroskopowe, mikroskopowe, termiczne i przeciwbakteryjne. Nanokompozyt chitozan/zeolit/ZnO może być stosowany jako skuteczny związek antybakteryjny w różnych zastosowaniach ze względu na swoją strukturalne i właściwości antybakteryjne.

Słowa kluczowe: ludzkie zdrowie, działanie antybakteryjne, nanokompozyty, chitozan, zeolit, tlenek cynku.

According to WHO statistics, the increase in bacterial resistance, which affects health and poses a significant financial burden to the world economy, is one of the most serious challenges to the treatment and healthcare system in this century [1]. Dental caries is a chronic, dynamic, and episodic disease that develops when a biofilm forms on a rigid structure and is influenced by several variables, including the presence of sugar substances (saccharides), the quality of saliva secretion and the passage of time. The acid produced by the biofilm damages and demineralized the tooth structure [2]. Despite the improvement in the quality of life and the establishment of preventive protocols, poor adherence to oral hygiene remains one of the main causes of tooth loss, which can have a negative impact on the physical and emotional well-being of people and be associated with significant economic consequences [3, 4]. *S. mutans* can have a cryogenic effect by consuming the delicate balance of regular oral flora, although it is usually present in the normal oral microbiota, especially in the pits and crevices of the tooth crown. During anaerobic metabolism, S. mutans and other bacteria in the oral flora ferment sugars and form lactic acid, which mineralizes enamel, dentin, and dental cementum [5]. Recent studies indicate that nanotechnology may offer new approaches to the prevention and treatment of dental caries, particularly in the management and control

[1)] Division of Dental Biomaterials, School of Dentistry, Kermanshah University of Medical Sciences, Kermanshah, Iran.

[2)] Advanced Dental Science and Technology Research Center, School of Dentistry, Kermanshah University of Medical Sciences, Kermanshah, Iran.

[3)] Department of Oral and Maxillofacial Medicine, School of Dentistry, Kermanshah University of Medical Sciences, Kermanshah, Iran.

[4)] Faculty of Health and Life Sciences, INTI International University, Nilai 71800, Malaysia.

[5)] Students Research Committee, Kermanshah University of Medical Sciences, Kermanshah, Iran.

[*)] Author for correspondence: fallahnianima@gmail.com

of dental plaque biofilm [6]. Nanomaterials are 100 nm in diameter or less, and in recent years there has been a significant increase in the use of their unique anti-infective properties [7, 8]. Material properties (hardness, active surface area, chemical reactivity, biological activity, and antimicrobial properties) change significantly as the particle size decreases from micrometers to nanometers and can be used in pharmaceutical, diagnostic, and disease management industries [9, 10].

Chitosan is made commercially by deacetylating chitin [11]. Due to the presence of active amino and hydroxyl groups in the polymer matrix, this biopolymer exhibits distinct polycationic and antibacterial characteristics [12]. Chitosan is highly effective at inhibiting bacterial growth while barely harming mammalian cells [13].

Numerous studies have been conducted on zinc oxide nanoparticles (ZnO NP_S) because of their exceptional electrical, chemical, optical, antifungal, and antibacterial characteristics. Several methods can be used to create ZnO nanoparticles with ease. Compared to many other metal oxides, zinc oxide (ZnO) has the potential to be biocompatible and has demonstrated several exceptional qualities in the biomedical and antibacterial application domains [14].

Aluminosilicates have received attention in different sectors due to their special properties. Zeolites are a group of aluminosilicates [15, 16]. Zeolite is a mineral compound with a stable porous crystal structure and numerous tiny holes among the crystals. This material has antibacterial, anti-caries, and biocompatibility properties, which can effectively treat periodontitis, help heal and regenerate tissue, and be used in most routine dental treatments [17]. Taguchi method, based on static methods and with actual performance, can provide a favorable condition for designing and synthesizing materials with a substantial standard [18, 19].

The aim of this study was to synthesize a novel chitosan/zeolite/ZnO nanocomposite and investigate its antibiofilm activity against the oral pathogen *S. mutans*.

EXPERIMENTAL PART

Synthesis of ZnO nanoparticles

The molten salt method was used for the synthesis of ZnO nanoparticles. For this purpose, 83 g of zinc chloride salt, 1.19 g of sodium hydroxide, and 1.1 g of potassium hydroxide were mixed and placed in the oven for 45 min under a temperature of 220°C, which is higher than the eutectic temperature of sodium and potassium. Then the obtained product was cooled at room temperature, washed three times with hot distilled water, and centrifuged to remove impurities and alkali metal salts. The sediment resulting from the centrifugation process was placed in an oven at 100°C for 2 h to remove its moisture and obtain the white powder of ZnO nanoparticles [20].

Synthesis of chitosan/zeolite/ZnO nanocomposites

For the synthesis of the studied nanocomposite ZnO nanoparticles were prepared using molten salt. Zeolite and chitosan polymer were provided commercially. Using the Taguchi method to figure out the best way to make this nanocomposite with the most antibacterial activity, nine experiments containing different ratios of chitosan (2.5, 5, and 7.5 mg/mL), zeolite (0.2, 0.4, and 0.6 mg/mL) and ZnO (3, 6, and 9 mg/mL) were designed. For this purpose, nine different nanocomposites were synthesized by using in situ method and different levels of chitosan polymer, ZnO nanoparticles, and zeolite to check their antibacterial power. In order to generate homogenous solutions, solutions with varied concentrations of the researched components were created in separate containers, magnetically stirred for 45 min, and then treated to ultrasound for 15 min. Containers containing chitosan solution were placed on a magnetic stirrer, and ZnO and zeolite nanoparticles solution was added little by little. A magnetic stirrer mixed the obtained solutions at 40°C for 60 min, then subjected them to ultrasonic waves for 15 min, and nanocomposites containing different ratios were formed. Then, the obtained solutions were placed in an oven at 60°C to become a nanocomposite powder.

Antibacterial activity

To investigate the antibacterial property of the synthesized chitosan/zeolite/ZnO nanocomposite against *S. mutans* biofilm, this bacterium (ATCC 35668) was prepared at the Iranian Industrial Microorganism Collection Center. To assess the antimicrobial property of nanocomposites, colony forming units (CFU) were used. Brain heart infusion medium (BHI) was used to prepare the bacterial suspension. One colony of *S. mutans* was incubated at 37°C for 48 h in a petri dish containing 5% defibrinated sheepblood and blood agar. Then, a suspension containing 0.5 McFarland (CFU/mL · 10^8) was prepared using double distilled water. Then 5 mL of the bacterial solution was added to 5 mL (150 μg/mL) of the synthesized nanocomposite in 9 experimental conditions. After that, the solutions were poured into the wells and shaken in a shaker incubator for 6 h at 37°C and 140 RPM. After collecting the suspension, it was serially diluted ten times. It was cultured for 24 h on a blood agar medium containing 5% defibrinated sheep blood at 37. After the bacteria had been cultured, the number of colonies was tallied and an average determined. There were three repetitions of the experiment, and the results were recorded [21].

Characterization

Multiple investigations were used to gauge the characteristics of the synthesized nanocomposite and its constituent parts. In this respect, various methods were used, such as Fourier-transform infrared spectroscopy

T a b l e 1. Taguchi design experiments and effects of chitosan/zeolite/ZnO synthesized nanocomposites on the survival rate of *Streptococcus mutans*

Experiment	Chitosan mg/mL	Zeolite mg/mL	ZnO mg/mL	Bacterial survival Log_{10} CFU/mL
1	2.5	0.2	3	2.64
2	2.5	0.4	6	2.07
3	2.5	0.6	9	1.24
4	5	0.2	6	0.93
5	5	0.4	9	0.32
6	5	0.6	3	1.39
7	7.5	0.2	9	0.00
8	7.5	0.4	3	1.74
9	7.5	0.6	6	0.68

(FT-IR) (Thermo Fisher Scientific, Waltham, MA,USA), X-ray crystallography (Philips X 'Pert (40kV, 30mA), Amsterdam, Netherlands),◎field emission scanning electron microscopy (FESEM) (MIRA III, TESCAN, Brno, Czech Republic), energy-dispersive X-ray spectroscopy (EDX) (MIRA III, TESCAN, Brno, Czech Republic), X-ray surface elemental mapping with SAMX detector (MIRA II, TESCAN, Brno, Czech Republic), transmission electron microscopy (TEM) (Philips EM208S, Amsterdam, Netherland), ultraviolet-visible spectroscopy (UV-Vis) (UV-160 A, Shimadzu, Kyoto, Japan), and thermogravimetric analysis (TGA and DTA) (Q600, TA Instruments, New Castle, DE, USA).

RESULTS AND DISCUSSION

Nine experiments based on the Taguchi method were designed to find the optimal conditions for manufacturing chitosan/zeolite/ZnO nanocomposite with the best antibacterial activity. Then, the viability of *S. mutans* strain was evaluated for the effect of synthetic nanocomposites under different conditions (Table 1). According to the results, the nanocomposite associated with experiment No. 7, which was created under the conditions of 7.5 mg/mL chitosan, 0.2 mg/mL zeolite and 9 mg/mL ZnO, has the strongest antibacterial activity against *S. mutans* biofilm. In its presence, the bacterial survival rate reached the lowest value, 0 CFU/mL.

The size, composition, crystallinity, and shape of nanoparticles like ZnO and silver help to define their intrinsic qualities. Their chemical, mechanical, electrical, structural, morphological, and optical properties can alter when their size is reduced to the nanoscale. The physical transit of nanoparticles into cellular structures is facilitated by these changed features, which enable nanoparticles to interact with biological cell components in a distinctive way [22]. In numerous investigations, ZnO nanoparticles and compounds using it have demonstrated considerable antibacterial activity against various bacterial species [23]. Reactive oxygen species, which can assault protein and lipid structures, enter the bacterial cytoplasm, and damage DNA, are produced as one of its processes.

Table 2 displays the results of a study examining the effect of chitosan, zeolite, and ZnO on the viability of *S. mutans* biofilm. The results showed that the third level in all three factors studied had the greatest effect on reducing the viability of *S. mutans*.

T a b l e 2. The main effects of different levels of chitosan, zeolite and ZnO on the survival rate of *Streptococcus mutans*

Factors	Level 1	Level 2	Level 3
Chitosan	1.98	0.88	0.81
Zeolite	1.19	1.38	1.10
ZnO	1.92	1.23	0.52

Table 3 illustrates how various variables interact to affect the likelihood that *S. mutans* bacteria will survive. The interaction impact of the first level of zeolite and the third level of ZnO on the survival of *S. mutans* bacteria each had a value of 38.63. Interactions between chitosan and ZnO at the third level were on the decrease in survival of *S. mutans* bacteria, with a value of 2.08. The interaction impact of the first level of chitosan and the second level of ZnO on the survival of *S. mutans* bacteria each had a value of 0.75.

T a b l e 3. The interactions effects of studied factors on the survival rate of *Streptococcus mutans*

Interacting factor pairs	Column	Severity index, %	Optimum conditions
Zeolite × ZnO	2×3	38.63	(1,3)
Chitosan × ZnO	1×3	2.08	(3,3)
Chitosan × Zeolite	1×2	0.75	(3,1)

The variables that affect the *S. mutans* bacteria survival rate are shown in a variance analysis in Table 4. ZnO nanoparticles had a 51.11% effect on the viability of *S. mutans* bacteria, followed by chitosan with a 45.04% effect and zeolite with a 1.45% effect.

T a b l e 4. Analysis of variance of factors affecting the survival rate of *Streptococcus mutans*

Factors	DOF*	Sum of squares	Variance	F-Ratio, F	Pure Sum	Percent, %
Chitosan	2	2.61	1.30	76.24	2.57	45.04
Zeolite	2	0.12	0.06	3.42	0.08	1.45
ZnO	2	2.95	1.48	86.38	2.92	51.11

*DOF – degree of freedom.

Based on the results of data analysis and the study of the influence of individual components and their mutual development, the optimal conditions for the synthesis of chitosan/zeolite/ZnO nanocomposite with maximum antibacterial properties were estimated. (Table 5). In this regard, ZnO and zeolite showed the highest and lowest contribution to the survival rate of *S. mutans* bacteria, respectively. Chitosan affected these two factors. When considering all factors, the third level was found to be optimal. It was determined that under ideal conditions, the synthesized nanocomposite totally inhibits the formation of *S. mutans* biofilm.

T a b l e 5. The optimum conditions for the synthesis of chitosan/zeolite/ZnO nanocomposites with the highest antibacterial activity

Factors	Level	Contribution
Chitosan	3	0.42
Zeolite	3	0.12
ZnO	3	0.70
Total contribution from all factors		1.24
Current grand average of performance		1.22
Bacterial survival at optimum condition		-0.02

FT-IR analysis

Figure 1 shows the FT-IR spectra of chitosan/zeolite/ZnO nanocomposite and its components in the wavelength range of 400–4000 cm^{-1}. The peak observed in the chitosan spectrum (Fig. 1a) in the zone 3271 to 3357 cm^{-1} is attributed to the stretching of N-H or O-H groups, and in 2856 cm^{-1} to the stretching of C-H groups. The peak in the zone 1639 cm^{-1} is associated with the vibrations of carbonyl bonds (C=O) (amide I) O=C-NHR. The absorption peak at 1579 cm^{-1} indicates the bending of N-H. These bonds are (amide II) (NH_2) [24].

In the spectrum shown in Fig. 1b, the observed peaks are located at 1057 cm^{-1}, 793 cm^{-1} and 467 cm^{-1}, which indicates the internal vibrations of Si-O-Si and Si-O-Al bridges in the zeolite. The peaks observed in the zone of 1637 cm^{-1} and between 3200 cm^{-1} and 3700 cm^{-1} in the zeolite are due to water absorbed by the zeolite [25]. The FT-IR spectrum of ZnO nanoparticles (Fig. 1c) shows a significant absorption peak at 3420 cm^{-1}, which is related to O-H bonds. The band near 1448 cm^{-1} is due to moisture absorption in the form of H-O-H bending vibrations. The absorption band at 452 cm^{-1} corresponds to the stretching vibrations of Zn-O [26]. The spectrum of the synthesized nanocompos-

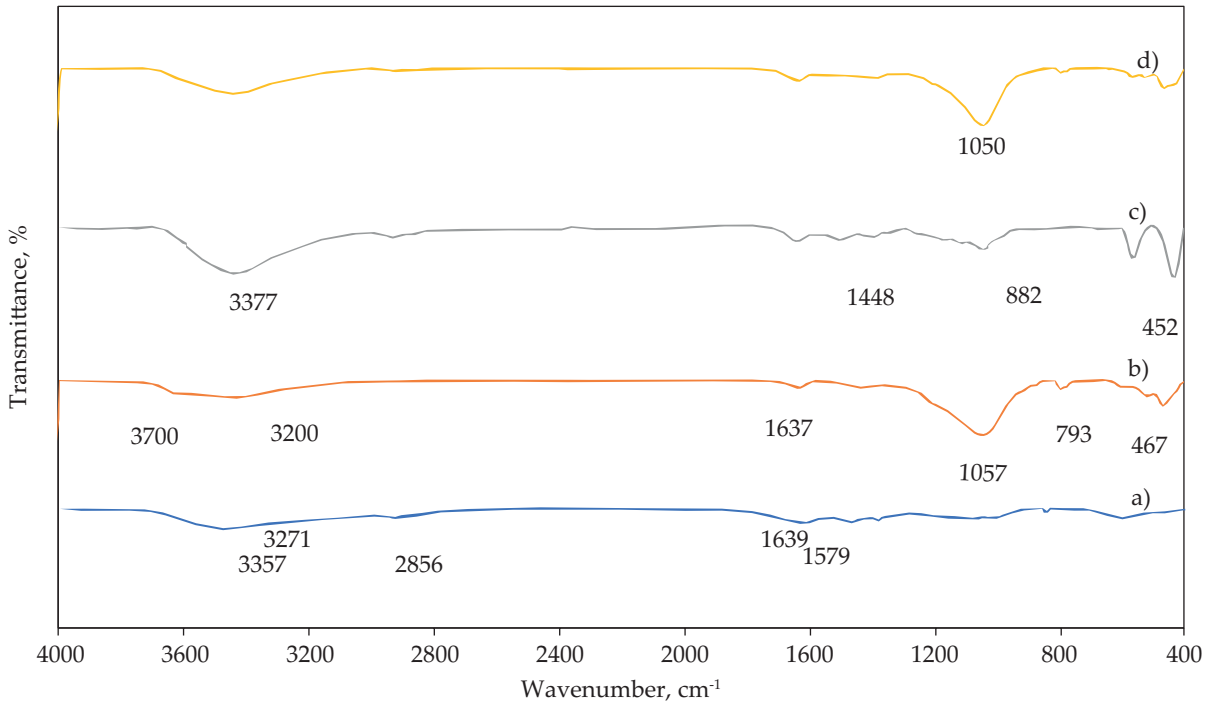

Fig. 1. FT-IR spectra: a) chitosan, b) zeolite, c) ZnO NPs, d) chitosan/zeolite/ZnO composite

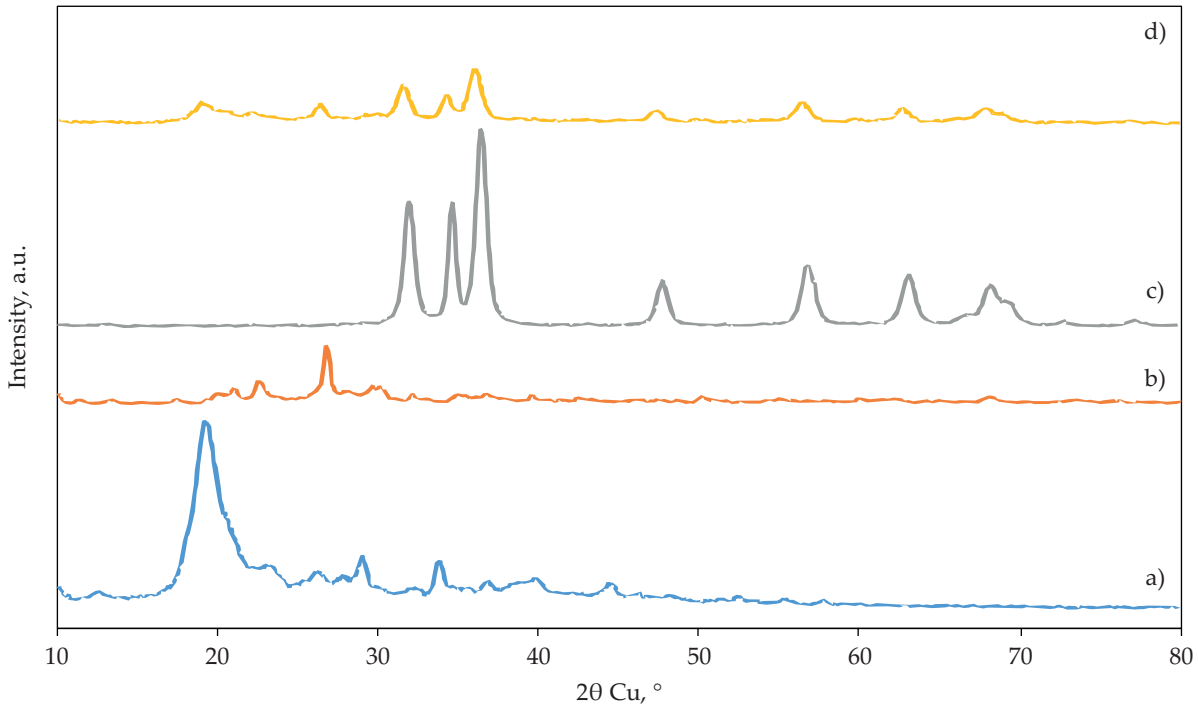

Fig. 2. XRD patterns: a) chitosan, b) zeolite, c) ZnO NPs, d) chitosan/zeolite/ZnO nanocomposite

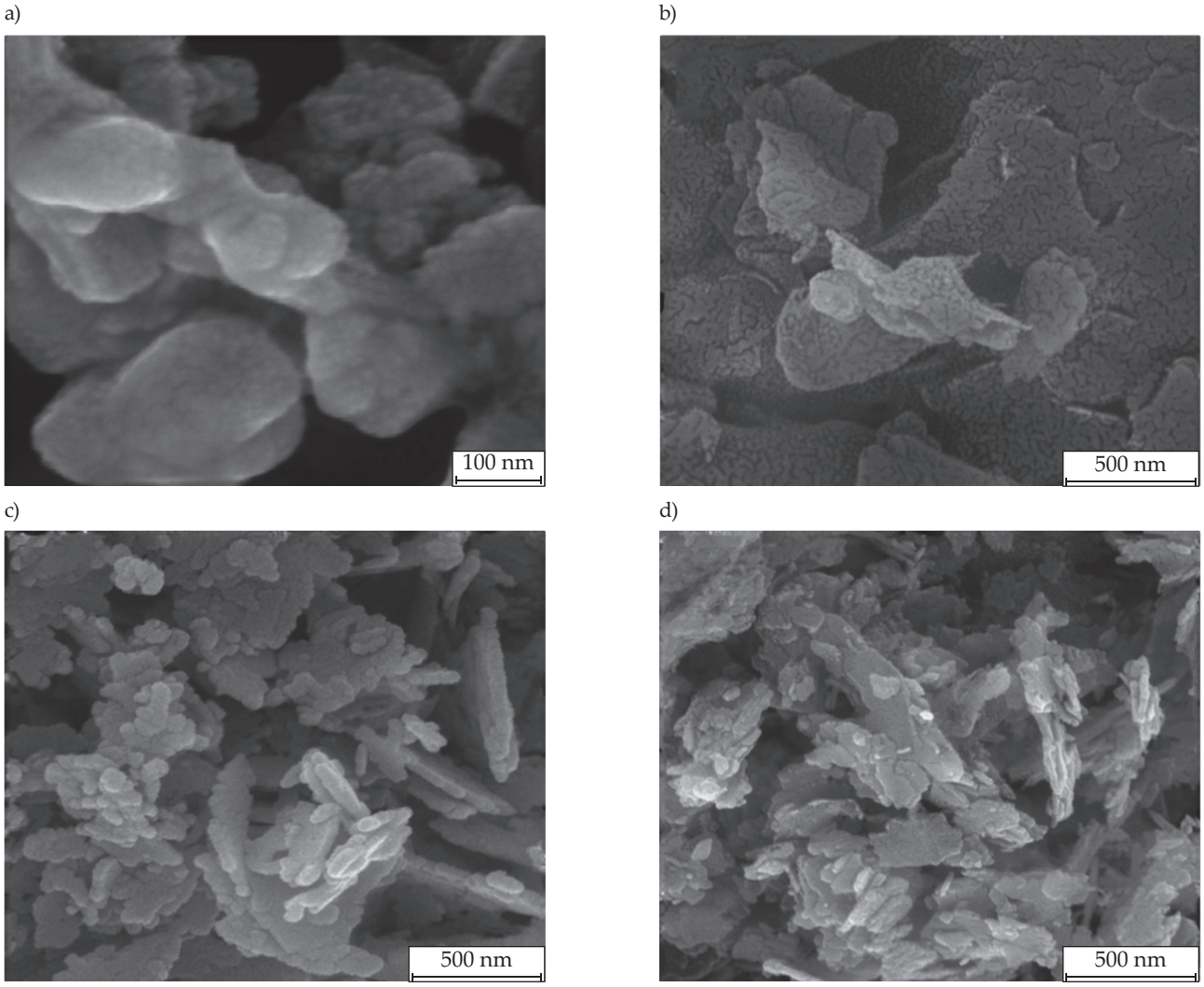

Fig. 3. SEM images: a) chitosan, b) zeolite, c) ZnO NPs, d) chitosan/zeolite/ZnO nanocomposite

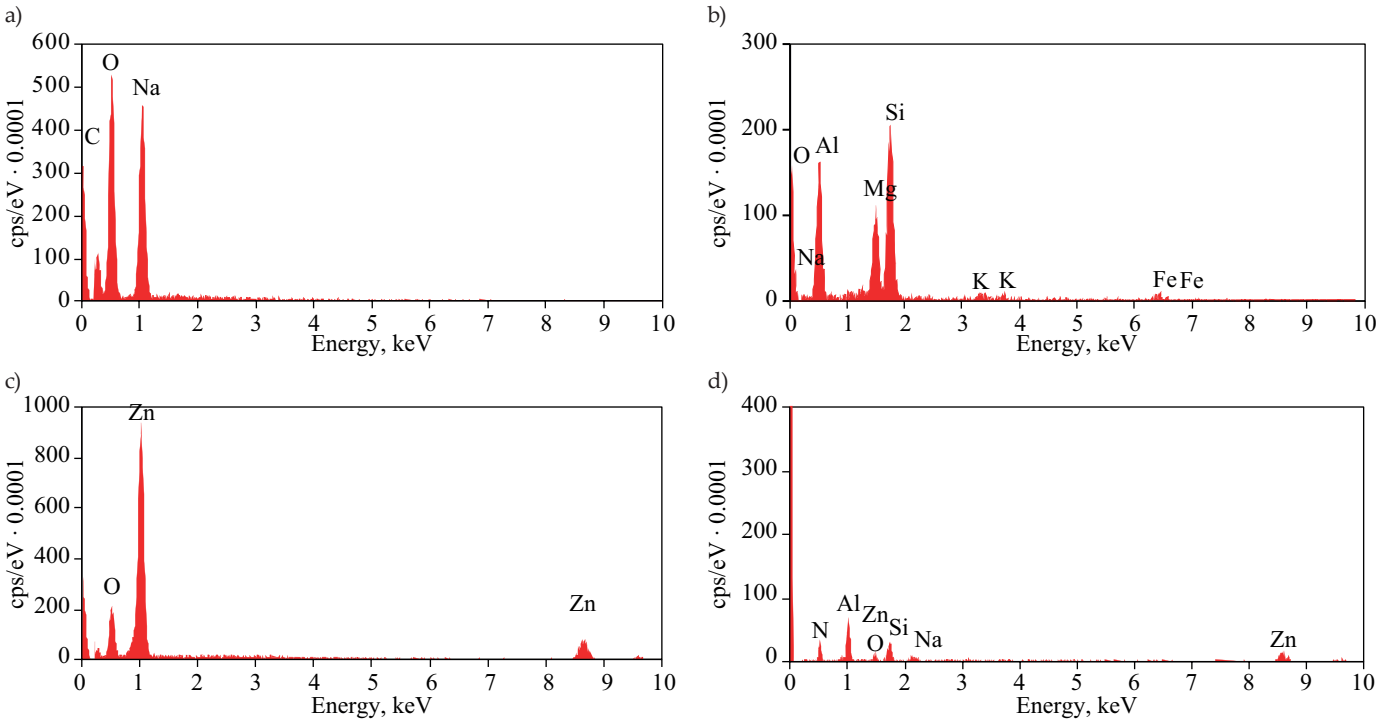

Fig. 4. EDX patterns: a) chitosan, b) zeolite, c) ZnO NPs, d) chitosan/zeolite/ZnO nanocomposite

ite is influenced by the zeolite component and resembles a zeolite graph.

XRD analysis

Fig. 2 shows the results of an X-ray diffraction investigation into the phase development and crystallography of the produced nanocomposite and its components. Sharpie peak was visible in the XRD pattern of chitosan nanoparticles at the 2θ diffraction angle of 19 degrees. This peak's existence and other peaks of lesser intensity demonstrated the crystalline nature of chitosan nanoparticles [27].

Pattern b (Fig. 2) shows the XRD pattern of zeolite, that zeolite peaks were observed at 2θ angles of 31, 33, 34, 42, 43, 44, 47, 48, 50, 52, 54, 57, 58, 59, 67, 71, and 73 degrees. This pattern is similar to the Tracy and Higgins report and Rowland and Higgins's results for a set of simulated powder XRD patterns for zeolites [28]. Figure 2c presents the XRD diffraction peaks that were consistent with wurtzite ZnO from the standard card (JCPDS 76-0704). Thus, the XRD pattern shows ZnO nanoparticles with fine hexagonal crystal structure, consistent with this reference file, except for ZnO. No characteristic diffraction peak was observed, which shows that nanoparticles are free from phase impurities and have high purity [29].

SEM analysis

SEM images presented in Fig. 3 confirm the appropriate size of the synthesized samples. Agglomeration of ZnO nanopowder is clearly seen in Fig 3c. In the synthesized nanocomposite, it was observed that ZnO nanoparticles were dispersed in the polymer network of chitosan and zeolite clay (Fig. 3d).

EDX analysis

Using X-ray energy diffraction spectroscopy, the components elements of samples of chitosan biopolymer, zeolite nanoparticles, ZnO nanoparticles, and chitosan/zeolite/ZnO nanocomposite were identified (Figure 4). These results showed differences in the Using X-ray energy diffraction spectroscopy, the components elements of samples of chitosan biopolymer, zeolite nanoparticles, ZnO nanoparticles, and chitosan/zeolite/ZnO nanocomposite identified elements of these compounds. Figure 4a displays the findings of the EDX elemental analysis of the chitosan biopolymer. X-ray energy diffraction spectroscopic analysis of this material's diffraction pattern indicated that 26.83% of its mass is composed of carbon, 52.67 % of its mass is oxygen, and 20.5 % of its mass is sodium. X-ray energy diffraction pattern of zeolite (Fig. 4b) revealed the existence of the elements, potassium (0.61 wt%), iron (2.82 wt%), aluminum (11.38 wt%), oxygen (59.37 wt%), and magnesium (0.83 wt%) and silicon (24.38 wt%). According to the ZnO nanoparticles X-ray energy diffraction pattern Fig. 4c, oxygen elements were present in weight percentages of 33.56% and 66.44%, respectively. Additionally, the synthesized nanocomposite's X-ray energy diffraction pattern in Figure 4d revealed a combination of the elements of the constituent part, resulting in a structure that con-

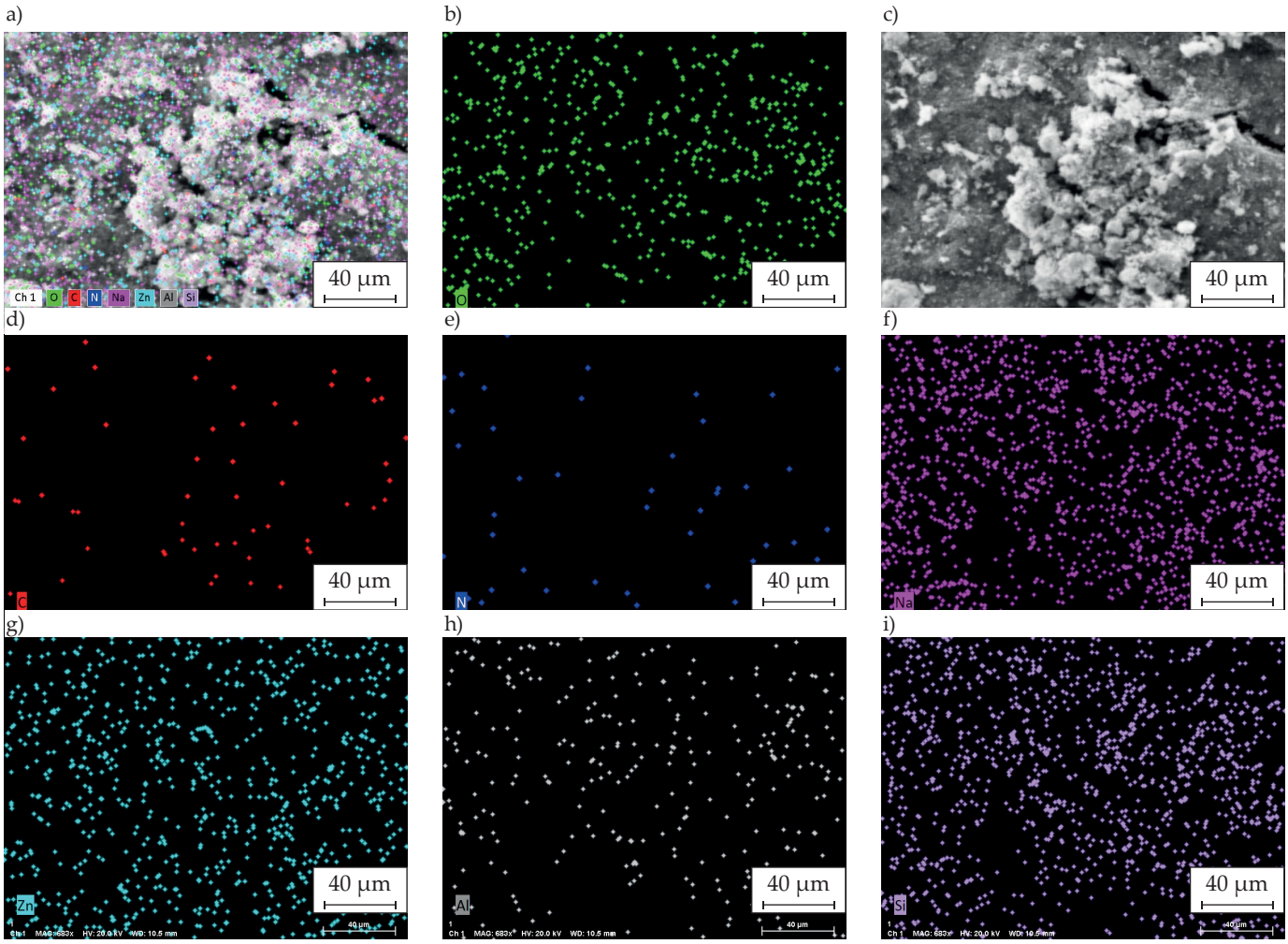

Fig. 5. Dispersion map of the composite components on the surface: a) nanocomposite, b) all elements, c) oxygen, d) carbon, e) nitrogen, f) sodium, g) zinc, h) aluminum, i) silicon

tained the elements: zinc (24.65 wt%), oxygen (15.12 wt%), silicon (5.48 wt%), carbon (4.20 wt%), sodium (2.86 wt%), aluminum (2.46 wt%), and nitrogen (0.33 wt%).

X-ray map analysis

Figure 5 displays the distribution map of the chitosan/zeolite/ZnO nanocomposite surface elements. This image demonstrates the equal distribution of aluminum, sodium, oxygen, nitrogen, zinc, carbon, and silicon across the overall structure of the synthesized nanocomposite and verifies its synthesis.

TEM analysis

The shape of the chitosan/zeolite/ZnO nanocomposite was investigated by preparing a TEM micrograph of the synthetic nanocomposite. Analysis of TEM micrographs revealed the creation of this nanocomposite (Fig. 6). ZnO and zeolite nanoparticles, which were integrated into the matrix structure and led to the formation of the chitosan/zeolite/ZnO nanocomposite, are small, black, and spherical particles.

UV–Vi's analysis

Fig. 7 depicts the UV-Vis absorption spectrum of chitosan/zeolite/ZnO nanocomposite and that of each of its components from 200 to 800 nm. The maximum absorption wavelength in the chitosan polymer (Fig. 7a) spectra was around 207 nm [30]. The wide particle size range

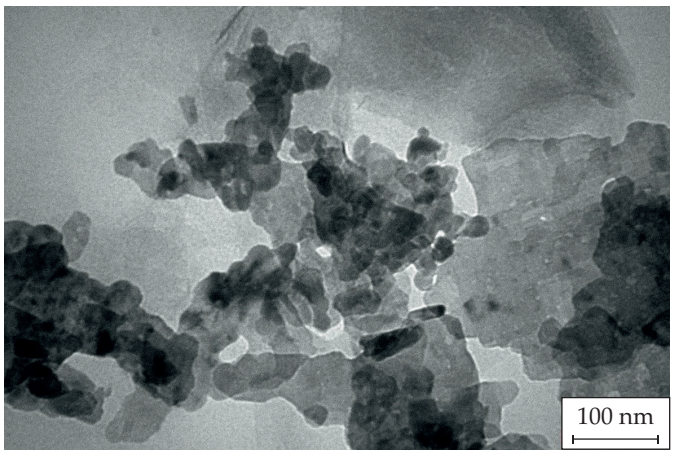

Fig. 6. TEM image of chitosan/zeolite/ZnO nanocomposite

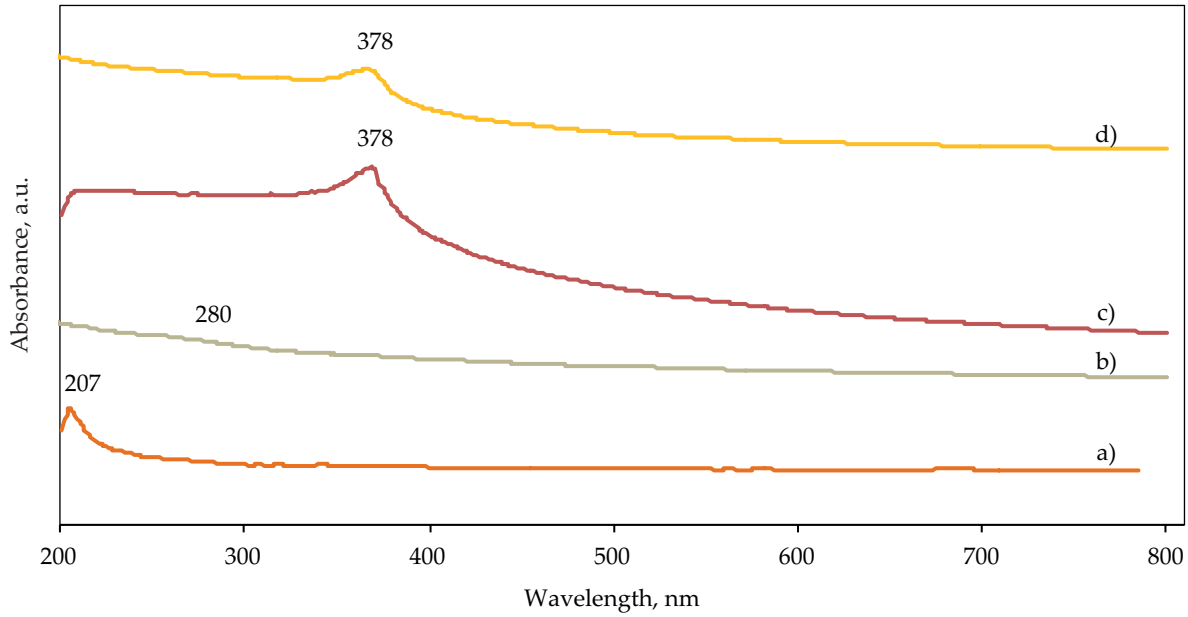

Fig. 7. UV-Vi's spectra: a) chitosan, b) zeolite, c) ZnO NPs, d) chitosan/zeolite/ZnO nanocomposite

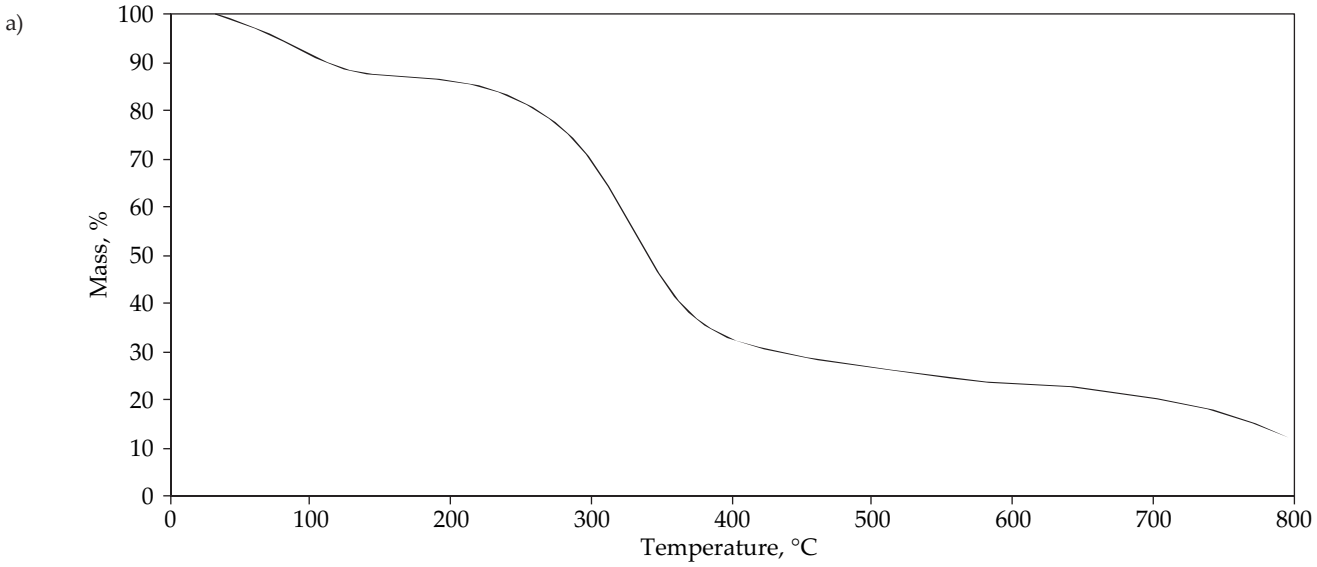

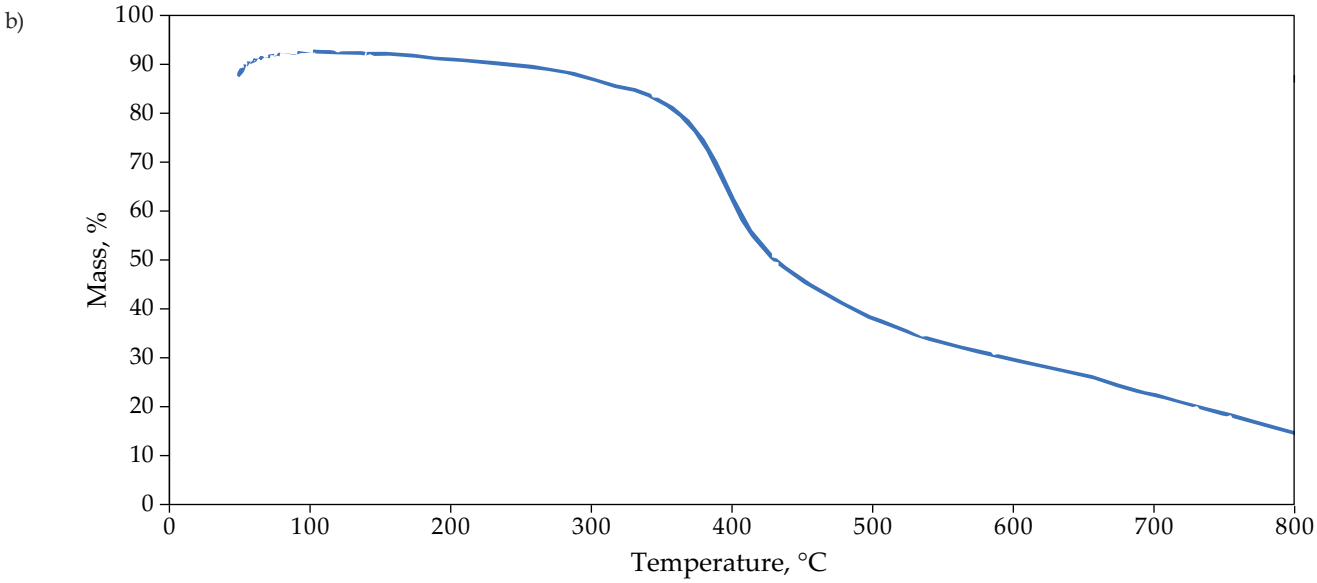

Fig. 8. TGA curves: a) chitosan, b) chitosan/zeolite/ZnO nanocomposite

for the zeolite can be attributed to the broad absorption band at 280 nm in plot (Fig. 7b) [31]. Fig. 7c displays the ZnO nanoparticle's UV-visible absorption spectrum [32]. The characteristic peak for ZnO hexagonal wurtzite is the absorption peak at 378 nm. In addition, the placement of ZnO nanoparticles in the context of nanocomposite was observed in the UV-Vis absorption spectrum (Fig. 7d), which also supported the development of nanocomposite.

Thermal analysis

To investigate its thermal properties, a TGA analysis was used to evaluate the chitosan/zeolite/ZnO nanocomposite. The TGA curve of chitosan (Fig. 8a) revealed two stages of weight loss between 47 and 450°C. With a weight loss of around 9%, the first stage was caused by the loss of water molecules between 47 and 100°C. Chitosan began structurally disintegrating around 247°C and decomposed at roughly 330°C with a weight loss of about 34% [33].

As seen in the TGA curve, the nanocomposite undergoes three distinct phases of weight loss between 25 to 800°C (Fig. 8b). A weight loss of roughly 7% was seen in the first stage, which ran from 25 to 224°C, while a loss of 17% was seen in the second stage, which ran from 225 to 425°C. A weight loss of 12% was seen in the third stage at temperatures between 430 and 800°C. The loss of physically adsorbed water causes the heat peak at 114°C in the first range (25–224°C) of TGA curves [34]. While the heat peaks in the second and third ranges at 250–400 and 500–898°C are connected to the degradation of polymer chains and chitosan, respectively [35].

CONCLUSIONS

Chitosan/zeolite/ZnO nanocomposite was successfully synthesized *in situ* by Taguchi method. The composite (7.5 mg/mL chitosan, 0.2 mg/mL zeolite and 9 mg/mL ZnO) obtained under optimal conditions shows good antibacterial properties against *S. mutans bacteria* and can be used as an antibacterial product in the pharmaceutical industry, in medicine and dentistry, in synthesis and diagnostics. To evaluate its effectiveness as a mouthwash against pathogenic bacteria, gingivitis and other infections-related disorders in the oral cavity, laboratory tests against fungi, animal studies and clinical trials are recommended.

ACKNOWLEDGMENTS
The authors gratefully acknowledge the Research Council of Kermanshah University of Medical Sciences for financial support.

Authors contribution
M.M.A. – conceptualization, methodology, validation, formal analysis, investigation, writing-original draft, writing-review and editing; D.B – conceptualization, methodology, validation, formal analysis, investigation, writing-original draft, writing-review and editing; N.A. – investigation, visualization, writing-original draft; A.A.A – methodology, formal analysis, investigation; T.E.B. – conceptualization, supervision, writing-original draft, editing.

Funding
The authors gratefully acknowledge the Research Council of Kermanshah University of Medical Sciences for financial support.

Conflict of interest
The authors declare no conflict of interest.

REFERENCES

[1] Eleraky N. E., Allam A., Hassan S. B. *et al.*: *Pharmaceutics* **2020**, *12(2)*, 142. https://doi.org/10.3390/pharmaceutics12020142
[2] Machiulskiene V., Campus G., Carvalho J. C. *et al.*: *Caries Research* **2020**, *54(1)*, 7. https://doi.org/10.1159/000503309
[3] Fraihat N., Madae'en S., Bencze Z. *et al.*: *International Journal of Environmental Research and Public Health* **2019**, *16(15)*, 2668. https://doi.org/10.3390/ijerph16152668
[4] Frazão P.: *Brazilian Oral Research* **2012**, *26*, 108. https://doi.org/10.1590/S1806-83242012000700016
[5] Cherukuri G., Veeramachaneni C., Rao G. *et al.*: *Journal of Conservative Dentistry* **2020**, *23*, 544. https://doi.org/10.4103/JCD.JCD_402_20
[6] Hannig M., Hannig C.: *Nature Nanotechnology* **2010**, *5*, 565. https://doi.org/10.1038/nnano.2010.83
[7] Safaei M., Taran M., Jamshidy L. *et al.*: *International Journal of Biological Macromolecules* **2020**, *158*, 477. https://doi.org/10.1016/j.ijbiomac.2020.04.017
[8] Taran M., Etemadi S., Safaei M.: *Journal of Applied Polymer Science* **2017**, *134*, 44613. https://doi.org/10.1002/app.44613
[9] Nazari M., Ebrahimzadeh F., Falaki M. *et al.*: *Nanomedicine Research Journal* **2022**, *7*, 19. https://doi.org/10.22034/nmrj.2022.01.002
[10] Nikolova M., Slavchov R., Nikolova G.: "Nanotechnology in Medicine" in "Drug Discovery

and Evaluation: Methods in Clinical Pharmacology" (edit. Hock F.J., Gralinski M.R.), Springer Nature Switzerland, Cham 2020. p. 533. https://doi.org/10.1007/978-3-319-68864-0_45
[11] Feliczak-Guzik A., Jadach B.,H. Piotrowska H. *et al.*: *Microporous and Mesoporous Materials* **2016**, *220*, 231. https://doi.org/10.1016/j.micromeso.2015.09.006
[12] Shahid-ul-Islam, B.S. Butola B.S.: *International Journal of Biological Macromolecules* **2019**, *121*, 905. https://doi.org/10.1016/j.ijbiomac.2018.10.102
[13] Choi C., Nam J.P., Nah J.: *Journal of Industrial and Engineering Chemistry* **2016**, *33*, 1. https://doi.org/10.1016/j.jiec.2015.10.028
[14] Raha S., Ahmaruzzaman M.: *Nanoscale Advances* **2022**, *4*, 1868. https://doi.org/10.1039/D1NA00880C
[15] Safaei M., Jafariahangari Y., Baharlouei A.: *International Journal of Agriculture and Biology* **2010**, *12*, 877.
[18] Safaei M., Boldaji F., Dastar B. *et al.*: *International Journal of Agriculture and Biology* **2012**, *14*, 299.
[17] Safari F., Houshmand B., Nejad A.E., *Regeneration, Reconstructio, and Restoration* **2020**, *3(4)*, 1. https://doi.org/10.22037/rrr.v3i4.24267
[18] Karna S.K., Sahai R.: *International Journal of Engineering and Mathematical Sciences* **2012**, *1*, 11.
[19] Safaei M., Taran M.: *International Journal of Biological Macromolecules* **2017**, *104*, 449. https://doi.org/10.1016/j.ijbiomac.2017.06.016
[20] Ghorbani F., Gorji P., Mobarakeh M.S. *et al.*: *Journal of Nanomaterials* **2022**, 7255181. https://doi.org/10.1155/2022/7255181
[21] Imani M.M., Kiani M., Rezaei F. *et al.*: *Ceramics International* **2021**, *47*, 33398. https://doi.org/10.1016/j.ceramint.2021.08.246
[22] Rasmussen J.W., Martinez E., Louka P. *et al.*: *Expert Opinion on Drug Delivery* **2010**, *7*, 1063. https://doi.org/10.1517/17425247.2010.502560
[23] da Silva B.L., Abuçafy M.P., Manaia E.B. *et al.*: *International Journal of Nanomedicine* **2019**, *14*, 9395.
[24] Kavaz D., Kirac F., Kirac M. *et al.*: *Journal of Biomaterials and Nanobiotechnology* **2017**, *8*, 203. https://doi.org/10.4236/jbnb.2017.84014
[25] Rachman R.A., Martia U.T.I., Aulia W. *et al.*: *AIP Conference Proceedings* **2018**, *2049*, 020073. https://doi.org/10.1063/1.5082478
[26] Zhao Z.Y., Wang M.H., Zhang H.P.: *Journal of Materials Science: Materials in Electronics* **2016**, *27*, 1777. https://doi.org/10.1007/s10854-015-3953-8
[27] Sharaf O.M., Al-Gamal M.S., Ibrahim G.A. *et al.*: *Carbohydrate Polymers* **2019**, *223*, 115094. https://doi.org/10.1016/j.carbpol.2019.115094
[28] Jahangirian H., Rafiee-Moghaddam R., Jahangirian N. *et al.*: *International Journal of Nanomedicine* **2020**, *15*, 1005. https://doi.org/10.2147/IJN.S231679
[29] Al-Kordy H.M.H., Sabry S.A., Mabrouk M.E.M.: *Scientific Reports* **2021**, *11*, 10924. https://doi.org/10.1038/s41598-021-90408-y
[30] Mohd Sultan N., Johan M.R.: *The Scientific World Journal* **2014**, *2014*, 84604. https://doi.org/10.1155/2014/184604
[31] Hu J., Xia F., Yang F. *et al.*: *RSC Advances* **2017**, *7*, 41204. https://doi.org/10.1039/C7RA06828J
[32] Wooten A.J., Werder D.J., Williams D.J. *et al.*: *Journal of the American Chemical Society* **2009**, *131*, 16177. https://doi.org/10.1021/ja905730n
[33] Sharmeen S., Rahman A.F.M.M., Lubna M.M. *et al.*: *Bioactive Materials* **2018**, *3*, 236. https://doi.org/10.1016/j.bioactmat.2018.03.001
[34] Moussout H., Ahlafi H., Aazza M. *et al.*: *Thermochimica Acta* **2018**, *659*, 191. https://doi.org/10.1016/j.tca.2017.11.015
[35] Pandiselvi K., Thambidurai S.: *Ionics* **2014**, *20*, 551. https://doi.org/10.1007/s11581-013-1020-0

Received 30 VIII 2024.
Accepted 13 IX 2024.

Rapid Communications

Przypominamy Autorom, że publikujemy artykuły typu **Rapid Communications – prace oryginalne wyłącznie w języku angielskim** (o objętości 4–5 stron maszynopisu z podwójną interlinią, zawierające 2–3 rysunki lub 1–2 tabele), którym umożliwiamy szybką ścieżkę druku (do 3 miesięcy od chwili ich otrzymania przez Redakcję). Artykuł należy przygotować wg wymagań redakcyjnych zamieszczonych we wskazówkach dla P.T. Autorów.

* * *

We remind Authors that we publish articles of the **Rapid Communications** type – **the original papers, in English only** (with a volume of 4-5 pages of double-spaced typescript, containing 2–3 figures or 1–2 tables), which allow a fast print path (up to 3 months from when they are received by the Editorial Board). The article should be prepared according to the editorial requirements included in the Guide for Authors.